Microstructure, Optical and Electrical Properties of Cu-Cu$_2$O Core-Shell Nanostructures

O. Mondal[*]

[1]Department of Physics, M.U.C Women's College, Burdwan, West Bengal, India

Abstract

Composites of nanometre-sized copper core–copper oxide (Cu-Cu$_2$O) shell with different diameters were synthesized by a facile one step co-solvent technique. By the analysis of X-ray diffraction (XRD) and transmission electron microscope (TEM) data, the resultant particles were confirmed to be pure and nanocrystalline in nature. The perfect core-shell structure of nanocrystalline Cu-Cu$_2$O was confirmed by using high resolution TEM. The presence of pure Cu and Cu$_2$O was further confirmed from optical absorbance spectrum and Fourier transform infrared (FT-IR) spectroscopy. The tailoring of position of optical absorption peaks, originating from Cu or Cu$_2$O nanoparticles, is possible by modulating the oil to water ratio, which controls the size of the composite particles and thickness of Cu$_2$O. Drastic change of electrical resistivity with change in thickness of shell, has been observed. Variation of resistivity with temperature delineates a semiconducting nature with two distinct activation processes. Results demonstrate that the activation energies for the core-shell nanostructure composites were found to be smaller than the bulk Cu$_2$O. Photoluminescence spectrum further confirms the semiconducting nature of the composite. In addition, the kinetic of core-shell morphology formation is also discussed briefly.

Keywords: Core shell nanocomposite; Co-solvent technique; Optical absorption; Electrical resistivity; Photoluminescence.

1. Introduction

Over the last two decades, controlled synthesis of different types of nanostructures has been mainly focused because of shape related properties [1-5]. Recently, many reports on applications of core-shell nanostructures in ultrahigh data storage media, optical, catalytic, biochemical and biomedical fields [6-9], have been found. Such structures often show a combination of the properties of the two (or more) materials involved, where the shell determines the surface properties of the particles, while the core is completely encapsulated by the shell [10-13]. The core-shell structure enhances the thermal and

---

[*] *Corresponding author*: oindrila.rng@gmail.com

chemical stability of the nanoparticles, improves solubility, makes them less cytotoxic and allows conjugation of other molecules to these particles [14,15].

It is well-known that metal nanoparticles can tune the catalytic properties of metal oxides [16-18]. However, in most of the catalytic studies, metal particles are usually deposited on the oxide surface [19]. These metal nanoparticles deposited oxide materials are also effective for CO oxidation, NO reduction, oxidation of hydrocarbon [20-22]. However, corrosion or dissolution of the metal nanoparticles after their extended exposure to reactants and the surrounding medium may pose a concern for their different activities. To solve this problem, a composite structure of metal nanoparticle core and oxide shell is being considered a better design because the oxide shell can protect the metal core and stabilize it against chemical attack.

Various synthesis procedures have been utilized in tailoring the metal-metal oxide core-shell nanostructures. Ghilane *et al.* [6] prepared Ag/Ag₂O core-shell nanostructure by heating commercially available Ag nanopowder in air atmosphere. Sun *et al*. [23] fabricated Zn/ZnO core-shell nanostructure by sputtering method. Seto *et al.* [10] developed a method to fabricate monodispersed Ni/NiO core-shell nanoparticles by pulsed laser ablation. Rahman *et al*. have prepared magnetic-polymer core-shell nanocomposites using two stage microemulsion techniques [24]. Microemulsion technique was also utilized in preparation of bimetallic core-shell nanocomposites [25]. The main idea behind the microemulsion technique is that by controlling the synthesis parameters appropriately one can use nanoreactors to produce tailor-made products down to a nanoscale level with new and special properties. The precise emphasis in the mechanisms is to control the particle size by controlling the proper microemulsion and the surfactant adsorption.

Cuprous oxide (Cu₂O) is a typical p-type direct band gap semiconductor with a band gap of 2.17 eV and has potential applications in electronics, solar energy conversion, sensors, and catalysis [26-29]. On the other hand, Cu nanoparticles possess unique catalytic, optical, and conducting properties [30-32]. To combine the properties of the two materials and prevent the oxidation of Cu nanoparticles, an attempt has been taken to synthesize core-shell nanostructure. Wang et al utilized a microemulsion technique to synthesize Cu-Cu₂O core-shell nanostructures using polyvinyl alcohol (PVA) as stabilizing agent [33]. Detailed structural characterization of Cu-Cu₂O core shell nanoparticles, synthesized using chemical reduction method in Kappaphycus alvarezii (K. alvarezii) media, is also reported by Khanehzaei *et al*. [34]. Ghodselahi *et al*. [35] reported synthesis of Cu-Cu₂O core-shell nanoparticles on the a-C:H thin films, prepared by co-deposition of RF-Sputtering and RF-PECVD. However, these studies were limited only to structural characterization. In this paper, we present a facile one step co-solvent technique of synthesizing Cu-Cu₂O core-shell nanostructures and investigate the change of electrical and optical properties with shell thickness. The innovative contribution of this work is the ability of prepare core-shell nanoparticles of controlled size and tunable optical properties. The electrical and optical properties are presented elaborately for Cu-Cu₂O core-shell nanoparticles prepared by co-solvent technique.

2. Experimental

2.1. *Materials*

Cupric nitrate [$Cu(NO_3)_2 \cdot 3H_2O$] and sodium hydroxide (NaOH), products of Merck (Germany) were used as precursors. Polyvinylpyrrolidone (PVP) was procured from Sigma-Aldrich (India). Commercially available analytical grade (AR) isopropyl alcohol from Sigma-Aldrich (India), was used without any further purification.

2.2. *Methods*

The $Cu-Cu_2O$ nanocomposite was synthesized by using a co-solvent based chemical reduction technique. The solvent system consisted of isopropyl alcohol and water stabilized by PVP. A saturated solution of $Cu(NO_3)_2 \cdot 3H_2O$ was prepared, added to isopropyl alcohol and stabilized using 0.1 g PVP under stirring. When the solution was clear, a calculated amount of sodium borohydride was added which resulted the solution to turn black indicating the completion of the reaction. The solution was centrifuged to collect the product which was further washed using water and ethanol to remove any unreacted ions. The washed products were dried in vacuum and used for further characterization. Three emulsion systems with different isopropyl alcohol to water ratios (R=200, 100, 50) were taken. The samples are named as S1, S2 and S3 respectively.

2.3. *Instrumentation*

The samples were characterized by powder X-Ray diffraction (XRD) using BRUKER D8 diffractometer equipped with graphite monochromaticized Cu radiation of wavelength 1.5418 Å, and operated at 40 kV voltage and 40 mA current. The microstructure and morphologies of the samples were further characterized with JEOL JEM2010 transmission electron microscope (TEM) operated at an accelerating voltage of 200 kV. The samples were dispersed in AR grade ethanol by ultrasonication and a drop of the dispersion was cast on a carbon coated copper grid for TEM study. The optical absorption spectra of nanoparticles of $Cu-Cu_2O$ core-shell were recorded on Cary 5000 UV-Vis-NIR spectrophotometer manufactured by AGILENT TECHNOLOGIES. The chemical structure of surface of the samples was characterized using Fourier Transform infra-red spectrum which was recorded on SHIMADZU FTIR 8400S spectrometer. Photoluminescence measurement was carried out on F-2500 FL spectrometer of HITACHI. The samples were cold pressed to pellets to perform electrical conductivity studies.

3. Results and Discussion

3.1. *Growth mechanism*

As the volume of water in solvent increased, it favoured the oxidation of Cu. A summary of the reactions taking place is given below

$$Cu^{++} \Rightarrow Cu^{+}$$

At this stage, two reactions are taking place simultaneously

  i) $Cu^{+} \Rightarrow Cu$

  ii) $Cu^{+} + OH^{-} \Rightarrow CuOH$

            $2CuOH \Rightarrow Cu_{2}O + H_{2}O$

Reaction (i) precedes reaction (ii) which favors the formation of Cu core surrounded by Cu$_2$O shell. In other word this leads to the enrichment of Cu$_2$O on the shell. The quantity of water in the solvent determines the percentage of Cu$_2$O phase and thus the thickness of the shell. The growth mechanism is schematically demonstrated in Fig. 1.
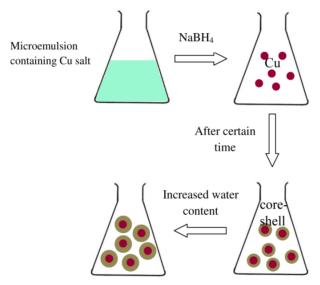

Fig. 1. Schematic presentation of Cu-Cu$_2$O core-shell formation.

3.2. *XRD study*

The powder X-ray diffraction pattern of the synthesized samples is shown in Fig. 2(a). From the XRD pattern the presence of two phases namely, Cu [JCPDS no 04-0836] and Cu$_2$O [JCPDS no 74-1230] are confirmed but they are found in different proportions. XRD pattern also confirms the purity of the composites as no extra peak is present.
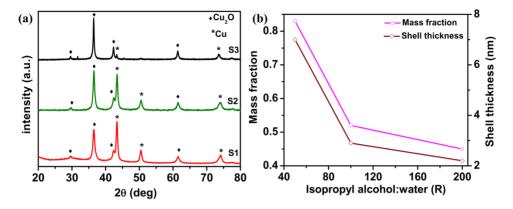
Fig. 2. (a) XRD pattern of the three samples. (b) Variation of mass fraction of Cu_2O and shell thickness with oil-water ratio (R).

As the presence of water in solvent system favours oxidation, increase in the amount of water in solvent, enhances the formation of Cu_2O. This is confirmed by the ratio of the intensity of the peaks of Cu_2O (I_{Cu2O}) and Cu (I_{Cu}) (considering the 100 % intense peak) in XRD study. The mass fraction of Cu in the composites can also be calculated from the relative ratio of 100 % intense peak of Cu (I_{Cu}) and Cu_2O (I_{Cu2O}) [36] using the relation (1)

$$Mass\ fraction\ of\ Cu\ phase = \frac{I_{Cu}}{I_{Cu}+I_{Cu2O}} \tag{1}$$

It can be seen from table 1 that mass fraction of Cu_2O increases from 0.45 to 0.83 as ratio of oil to water (R) decreases from 200 to 50. The thickness of shell for core-shell nanostructure can also be calculated theoretically from the volume fraction of the phase of the shell [37] using the relation (2),

$$V_{shell}/V_{total} = \left[\left(\frac{D}{2}\right)^3 - \left(\frac{D}{2}-t\right)^3\right] \Big/ \left(\frac{D}{2}\right)^3 \tag{2}$$

where, D is the core diameter, t is the shell thickness, V_{shell} is volume of shell. V_{shell} is calculated from mass fraction of the phase considering the density and D is obtained from Debye-Scherrer formula. The core diameter (size of Cu nanoparticles) was calculated using Debye Scherrer formula and the shell thickness obtained from relation (2) is presented in table 1. It is interesting to observe that the thickness of shell Cu_2O increases with decrease in R, keeping the size of Cu particle almost identical. The variations of volume fraction and shell thickness of Cu_2O, with the ratio R, are plotted in Fig. 2(b). We also made an attempt to calculate the lattice constant of the two different phases using the relation (3) for cubic structures

$$d_{hkl} = \frac{a}{\sqrt{h^2+k^2+l^2}} \tag{3}$$

The calculated values are presented in Table 1 and they match well with the standard value of Cu and Cu_2O.

Table 1. Analyzed results of XRD.

Sample name	Mass fraction of		Lattice constant a (Å)		Core size of Cu (nm)	Shell thickness of Cu_2O (nm)	Total diameter of particle (nm)
	Cu	Cu_2O	Cu	Cu_2O			
S1	0.55	0.45	3.608	4.257	16.2	2.1	20.6
S2	0.48	0.52	3.609	4.261	16	2.9	21.8
S3	0.17	0.83	3.614	4.263	18	7	32

3.3. *UV-Vis absorbance spectroscopy*

The optical absorption spectra of the samples dispersed in ethanol are presented in Fig. 3. It is clearly visible that an absorbance band in the range 470-510 nm is present in all the samples and a broad hump around 601 nm is present only in S1. The band between 470-510 nm is attributed to optical band gap of Cu_2O and that around 601 nm corresponds to surface plasmon resonance (SPR) of Cu nanoparticles in the core. The blue shift in the position of absorption band of Cu_2O (for bulk Cu_2O ~570 nm) is attributed to quantum confinement [34,38]. However, red shift in SPR of Cu compared to bulk Cu (~572 nm) and broadening of the peak, confirms the presence of a thin shell on Cu core [39], which in our case is of Cu_2O.
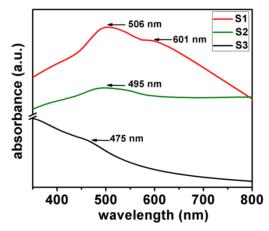

Fig. 3. Optical absorbance spectra of samples S1, S2 and S3 dispersed in ethanol.

Further, it is also observed that the plasmonic peak is totally suppressed in sample S3 that has maximum oxide content i.e. thicker shell. According to the suggestion of Mulvaney *et al.*, [40] monolayer of Au should be sufficient to mask the Ag plasmon resonance band completely. So, the above phenomenon could be due to the fact that the increased Cu_2O content on the surface resulted in the damping of the underlying Cu

surface plasmon band. This also proves the growth of Cu-Cu$_2$O core-shell nanostructure. The optical band gap of the composite was determined from the position of optical absorbance peak and is presented in Table 2. It is well known that the band gap decreases with increase in particle size, however, in our case the inverse variation of the band gap with size of Cu$_2$O occurs. Interestingly, we observe that the band gap decreases with increase in Cu content of the sample. Thus, the variation of band gap can be well explained with the consideration of the volume fraction of Cu core in the core-shell nanocomposite.

3.4. *Morphological study*

TEM provides the direct evidence of phases and particle size. The representative TEM image for sample S2 is presented in Fig 4(a), which reveals that particles are roughly spherical in nature and little agglomerated. Further, it is also visible (in Fig 4(a)) that a thin layer of PVP caps the particles and controls the growth. The analysis of the particle size histogram obtained from measurement of large number of particles using a log-normal distribution revealed the average size to be 12 nm with standard deviation of 1.25 nm (Fig. 4(b)). The high resolution TEM (HRTEM) image of sample S2 is presented in Fig. 4(c). The contrast between core and shell of nanoparticles is a direct proof of the core-shell structure of the synthesized composite with Cu core and Cu$_2$O shell (as illustrated by the difference in electron density). The particles are also highly crystalline as can be clearly seen from lattice fringes.
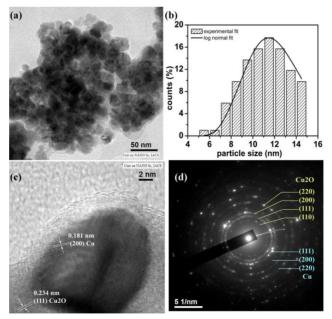

Fig. 4. (a) Transmission electron micrograph and (b) particle size distribution, (c) High resolution transmission electron micrograph and (d) SAED pattern, of sample S2.

The d-values calculated from lattice fringes in HRTEM further confirm that the constituent of core is Cu and that of shell is Cu$_2$O. The d value calculated from SAED pattern of the composite confirms the presence of both Cu and Cu$_2$O phases. The corresponding planes are labelled in Fig. 4(d). The result of morphological study using TEM is in good agreement with the result obtained from XRD and optical study.

3.5. *FT-IR spectroscopy*

The FTIR spectra of the as-grown samples were recorded to study the chemical structure and bondings present in the prepared core-shell structure. The FT-IR spectra of the samples in ordinary atmosphere and room temperature are presented in Fig. 5. The most prominent peaks correspond to symmetric ($\sim$2849 cm^{-1}) and anti-symmetric ($\sim$2922 cm^{-1}) stretching vibrations of –CH$_2$, stretching mode of -C=O ($\sim$1653 cm^{-1}) and stretching of C≡N bond ($\sim$1346 cm^{-1}). These bonds are characteristics of PVP which confirms its presence on the surface of the synthesized samples. The band $\sim$ 620 cm^{-1} is ascribed to the Cu-O bond of Cu$_2$O [41]. The intensity of this particular peak (Fig. 5.(b)) is found to be strongest for the sample S3 which indicates that it contains maximum Cu$_2$O that matches well with the XRD observation. It is clear from the magnified portion of the FTIR spectra (Fig. 5(b)) that the bond of CuO ($\sim$530 cm^{-1}) is absent in this case (marked with blue circle). In spite of the fact that Cu^{2+} is more stable than Cu$^+$, in our samples only Cu$_2$O phase is present which is clearly confirmed from IR spectra.
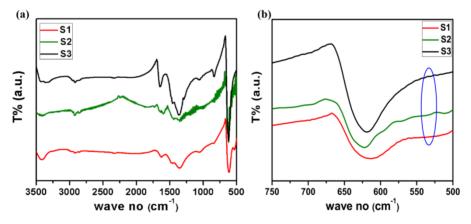

Fig. 5. (a) FT-IR spectra of sample S1, S2 and S3.(b) Magnified portion of the FTIR spectra.

3.6. *Photoluminescence properties*

Photoluminescence (PL) spectroscopy is a non-destructive method for probing the electronic structure of solid state materials. The room temperature photoluminescence spectra of the samples, with excitation of 425 nm, are presented in Fig. 6. The spectra of all the samples consist of two overlapping peaks within the range 550-625 nm, a green emission at 568 nm and an orange emission at 600 nm. The green emission corresponding

to the sharp peak ~568 nm in all the samples is attributed to near band-edge emission of Cu_2O [42]. The orange emission corresponding to the neck at 598 nm can be ascribed to oxygen vacancy (V_O) in the samples [43]. As the nanocomposites are photoluminescent, they can be used in various optical devices.
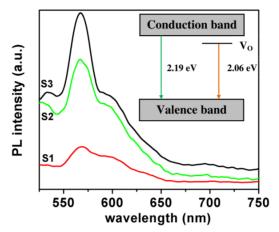

Fig. 6. Room temperature photoluminescence spectra of the samples.

3.7. *Electrical properties*

Fig. 7 shows the variation of resistivity as a function of inverse temperature for the three different samples. The resistivity variation of the samples can be ascribed to typical band conduction and it appears to be controlled by more than one thermally activated process. The activation energies were calculated from the slopes of the curves presented.
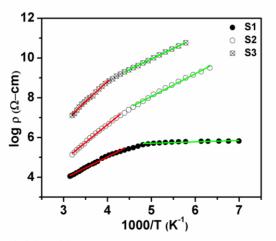

Fig. 7. Variation of resistivity with temperature.

The higher activation energy is attributed to conduction through bare copper oxide particles and the lower one to that through the copper nanocores. Table 2 summarizes the activation energy values obtained from electrical resistivity measurements. It is observed that the activation energy is smaller (~0.65 eV) than reported for bulk Cu_2O [44]. The 1st activation energy increases with increase of oxide phase. The semiconducting behavior exhibited by the latter rules out the possibility of any percolative metallic chain contributing to the transport behavior. As the Cu_2O shell coats the conductive Cu core, we strongly believe that electron tunneling occurs rather than percolation.

Table 2. Analyzed results of electrical and optical study.

Sample name	Activation energy (eV)		Position of absorption band (nm)	Band gap (eV)
	1st	2nd		
S1	0.2137	0.0103	506	1.21
S2	0.3374	0.2196	495	1.59
S3	0.3899	0.2111	475	2.62

4. Conclusion

In summary, we have successfully prepared nanostructured Cu metal core–Cu_2O shell through an elegant synthesis strategy. The particle size analysis by XRD and TEM studies confirm that the resultant materials were core-shell nanocomposite. Results indicate that the shell thickness could be controlled by the oil to water ratio in the solvent system. The UV-Vis spectra of nanocomposite showed distinct absorption peaks for the metal and oxide separately. It is to be noted here that the SPR of Cu nanoparticles is suppressed for thicker Cu_2O shell, rarely observed, when compared with available published literature. The resistivity variation of the samples can be ascribed to typical band conduction and it appears to be controlled by two distinct thermally activated processes. In addition, no semiconductor to metal transition is observed though the mass fraction of Cu metal was 55 %. The newness of this work is tunable size and optical properties of Cu-Cu_2O core-shell nanocomposites prepared by a one step facile co-solvent process. This low cost and easy method of preparation of Cu-Cu_2O core-shell nanocomposites may open possibilities of various applications in optical devices and catalytic activities.

References

1. E Carbó-Argibay, B Rodrαíguez-González, J. Pacifico, I. Pastoriza-Santos, J. Perez-Juste, and L. M. Liz-Marzán, Angew. Chem. Int. Ed. **46**, 8983 (2007). https://doi.org/10.1002/anie.200703259
2. X. Xu, and M. B. Cortie, J. Phys. Chem. C **111**, 18135 (2007). https://doi.org/10.1021/jp076425q
3. Q. Song and Z. J. Zhang, J. Am. Chem. Soc. **126**, 6164 (2004). https://doi.org/10.1021/ja049931r
4. M. -P. Pileni, Nat. Mater. **2**, 145 (2003). https://doi.org/10.1038/nmat817
5. L. Liu, H. -Z. Kou, W. Mo, H. Liu, and Y. Wang, J. Phys. Chem. B **110**, 15218 (2006). https://doi.org/10.1021/jp0627473
6. J. Ghilane, F. -R. F. Fan, and A. J. B. Dunwoody, Nano Lett. **7**, 1406 (2007). https://doi.org/10.1021/nl070268p
7. K. F. Huo, Z. Hu, J. J. Fu, H. Xu, X. Z. Wang, Y. Chen, Y. N. Lu, B. H. Liu, and J. Ding, J. Mater. Res. **18**, 1641 (2003). https://doi.org/10.1557/JMR.2003.0225
8. X. Teng, D. Black,N. J. Watkins, Y. Gao, and H. Yang, Nano Lett. **3**, 261 (2003). https://doi.org/10.1021/nl025918y
9. C. -C. Lee, and D. -H. Chen, Nanotechnology **17**, 3094 (2006). https://doi.org/10.1088/0957-4484/17/13/002
10. T. Seto, H. Akinaga, F. Takano, K. Koga, T. Orii, and M. Hirasawa, J. Phys. Chem. B **109**, 13403 (2005). https://doi.org/10.1021/jp052084+
11. H. Zeng, J. Li, Z. L. Wang, J. P. Liu, and S. Sun, Nano Lett. **4**, 187 (2004). https://doi.org/10.1021/nl035004r
12. G. Zhou, M. Lu, and Z. Yang, Langmuir **22**, 5900 (2006). https://doi.org/10.1021/la060339k
13. N. Li, W. Yan, W. Zhang, Z. Wang, and J. Chen, J. Mater. Chem. A **7**, 19324 (2019). https://doi.org/10.1039/C9TA05846J
14. Y. Chen, C. Zhu, and T. Wang Nanotechnology 17, 3012 (2006). https://doi.org/10.1088/0957-4484/17/12/033
15. Y. Wang, Q. Guo, S. Lin, B. Chen, and D. Zheng, J. Phys.: Conf. Series **152**, ID 012018 (2009). https://doi.org/10.1088/1742-6596/152/1/012018
16. C. T. Campbell, Science **306**, 234 (2004). https://doi.org/10.1126/science.1104246
17. S. Phadtare, A. Kumar, V. P. Vinod, C. Dash, D. V. Palaskar, M. Rao, P. G. Shukla, S. Sivaram, and M. Sastry, Chem. Mater. **15**, 1944 (2003). https://doi.org/10.1021/cm020784a
18. P. V. Kamat, J. Phys. Chem. B **106**, 7729 (2002). https://doi.org/10.1021/jp0209289
19. N. Zheng and G. D. Stucky, J. Am. Chem. Soc. **128**, 14278 (2006). https://doi.org/10.1021/ja0659929
20. R. Zanella, S. Giorgio, C-H. Shin, C. R. Henry, and C. Louis, J. Catal. **222**, 357 (2004).
21. M. M. Maye, Y. Lou, and C-J. Zhong, Langmuir 16, 7520 (2000). https://doi.org/10.1021/la000503i
22. I. Balint, A. Miyazaki, and K. Aika, Appl. Catal. B: Envir. **37**, 217 (2002). https://doi.org/10.1016/S0926-3373(01)00338-1
23. H. Sun and X. Pan, J. Mater. Res. **19**, 3062 (2004). https://doi.org/10.1557/JMR.2004.0402
24. M. M. Rahman, M. M. Chehimi, H. Fessi, and A. Elaissari, J. Colloid Interf. Sci. **360**, 556 (2011). https://doi.org/10.1016/j.jcis.2011.04.078
25. F. Barroso and C. Tojo, J. Colloid Interf. Sci. **363**, 73 (2011). https://doi.org/10.1016/j.jcis.2011.07.033
26. Y. Tan, X. Xue, Q. Peng, H. Zhao, T. Wang, and Y. Li, Nano Lett. **7**, 3723 (2007). https://doi.org/10.1021/nl0721259
27. L. -I. Hung, C. -K. Tsung, W. Huang, and P. Yang, Adv. Mater. **22**, 1910 (2010). https://doi.org/10.1002/adma.200903947
28. J. Zhang, J. Liu, Q. Peng, X. Wang, and Y. Li, Chem. Mater. **18**, 867 (2006). https://doi.org/10.1021/cm052256f

29. B. White, M. Yin, A. Hall, D. Le, S. Stolbov, T. Rahman, N. Turro, and S. O'Brien, Nano Lett. **6**, 2095 (2006). https://doi.org/10.1021/nl061457v
30. R. M. Crooks, M. Zhao, L. Sun, V. Chechik, and L. K. Yeung, Acc. Chem. Res. **34**, 181 (2001). https://doi.org/10.1021/ar000110a
31. Y. Wang, P. Chen, and M. Liu, Nanotechnology **17**, 6000 (2006). https://doi.org/10.1088/0957-4484/17/24/016
32. S. B. Kalidindi, U. Sanyal, and B. R. Jagirdar, Chem. Chem. Phys. **10**, 5870 (2008). https://doi.org/10.1039/b805726e
33. C. Y. Wang, Y. Zhou, Z. Y. Chen, B. Cheng, H. J. Liu, and X. Mo, J. Colloid Interf. Sci. **220**, 468 (1999). https://doi.org/10.1006/jcis.1999.6502
34. H. Khanehzaei, M. B. Ahmad, K. Shameli, and Z. Ajdari, Int. J. Electrochem. Sci. **10**, 404 (2015).
35. T. Ghodselahi, M. A. Vesaghi, A. Shafiekhani, A. Baghizadeh, and M. Lameii, Appl. Surf. Sci. **255**, 2730 (2008). https://doi.org/10.1016/j.apsusc.2008.08.110
36. A. Katasifaras and N. Spanos, J. Cryst. Growth **204**, 183 (1999). https://doi.org/10.1016/S0022-0248(99)00174-8
37. S. Aoyagi, Y. Kuroiwa, A. Sawada, H. Kawaj, and T. Atake. J. Therm. Anal. Calorim. **81**, 627 (2005). https://doi.org/10.1007/s10973-005-0834-z
38. K. Chatterjee, D. Das, and D. Chakravorty, J. Phys. D: Appl. Phys. **38**, 451 (2005). https://doi.org/10.1088/0022-3727/38/3/015
39. D. -H. Chen, and C. -J. Chen, J. Mater. Chem. **12**, 1557 (2002). https://doi.org/10.1039/b110749f
40. P. Mulvaney, M. Giersig, and A. Henglein, J. Phys. Chem. **97**, 7061 (1993). https://doi.org/10.1021/j100129a022
41. K. Borgohain, J. B. Singh, M. V. Rama Rao, T. Shripathi, and S. Mahamuni, Phys. Rev. B **61**, 11093 (2000). https://doi.org/10.1103/PhysRevB.61.11093
42. E. Ko, J. Choi, K. Okamoto, Y. Tak, and J. Lee, Chem. Phys. Chem. **7**, 1505 (2006). https://doi.org/10.1002/cphc.200600060
43. I. Tanaka, F. Oba, K. Tatsumi, M. Kunisu, M. Nakano, and H. Adachi, Mater. Trans. **43**, 1426 (2002). https://doi.org/10.2320/matertrans.43.1426
44. R. S. Toth, R. Kilkson, and D. Trivich, Phys. Rev. **122**, 482 (1961). https://doi.org/10.1103/PhysRev.122.482